Phase separation in hydrogen–helium mixtures at Mbar pressures

Miguel A. Morales[a], Eric Schwegler[b], David Ceperley[a,c,d,1], Carlo Pierleoni[d,e], Sebastien Hamel[b], and Kyle Caspersen[b]

[a]Department of Physics, [c]National Center of Supercomputing Applications, and [d]Institute of Condensed Matter Theory, University of Illinois at Urbana–Champaign, Urbana, IL 61801; [b]Lawrence Livermore National Laboratory, Livermore, CA 94550; and [e]Consorzio Nazionale Interuniversitario per le Scienze Fisiche della Materia and Physics Department, University of L'Aquila, Via Vetoio, I-67100 L'Aquila, Italy

Contributed by David Ceperley, December 11, 2008 (sent for review November 3, 2008)

The properties of hydrogen–helium mixtures at Mbar pressures and intermediate temperatures (4000 to 10000 K) are calculated with first-principles molecular dynamics simulations. We determine the equation of state as a function of density, temperature, and composition and, using thermodynamic integration, we estimate the Gibbs free energy of mixing, thereby determining the temperature, at a given pressure, when helium becomes insoluble in dense metallic hydrogen. These results are directly relevant to models of the interior structure and evolution of Jovian planets. We find that the temperatures for the demixing of helium and hydrogen are sufficiently high to cross the planetary adiabat of Saturn at pressures ≈5 Mbar; helium is partially miscible throughout a significant portion of the interior of Saturn, and to a lesser extent in Jupiter.

ab initio molecular dynamics | high pressure | planetary interiors

The two lightest elements, hydrogen and helium, are fascinating to physicists. Ubiquitous in the universe, their abundance ratio provide stringent checks on cosmological nucleosynthesis theories and the global distribution of hydrogen in the observable universe provides clues to the origin and large scale structures of galaxies. They are the essential elements of stars and giant planets. Yet, despite the seeming simplicity of their electronic structure, there are many unanswered questions about their fundamental properties, especially at high pressures. One such question is under what conditions are these elements miscible. The answer will have a crucial impact on our understanding of the evolution and the structure of the giant planets in our solar system and beyond.

Jupiter and Saturn, the simplest among the Jovian planets, are generally believed to have been formed approximately at the same time as the sun, although certain direct observations (such as Saturn's excess luminosity) appear to contradict this planetary formation theory. In addition to being mostly made of hydrogen and helium, a characteristic of Jovian planets is that they radiate more energy than they take in from the sun. Various models of their evolution and structure have been developed (1–4) to describe a relation between the age, volume, and mass of the planet and its luminosity. The current luminosity of Jupiter is well described with an evolution model for a convective homogeneous planet radiating energy left over from its formation 4.55 billion years ago. However, a similar model seriously underestimates the current luminosity of Saturn (5). Hence, either Saturn formed much later than Jupiter, or there is an additional energy source playing a more important role in Saturn than in Jupiter. In addition, the atmospheric abundance of helium in both Jupiter and Saturn appears to be lower than the accepted proto-solar values, more so in Saturn than in Jupiter (1).

Salpeter and Stevenson (6–9) proposed that helium condensation could be responsible for both the excess luminosity in Saturn and the helium depletion in the atmosphere of both Jovian planets. Suppose there is a region in the planet's interior where helium is insoluble; helium droplets will form and the denser helium will act as a source of energy, both through the release of latent heat, and by descending deeper into the center of the planet. Because Jupiter and Saturn have different total masses, the thermodynamic conditions in the planetary interiors could be such that this condensation process is more prevalent in Saturn than in Jupiter.

Previous attempts to calculate the immiscible temperature, as a function of pressure and helium concentration, by Stevenson (7), Straus *et al*. (10), Hubbard *et al.* (11), Klepeis *et al.* (12), and Pfaffenzeller *et al.* (13) led to inconsistent conclusions as to the importance of phase separation in the interiors of Saturn and Jupiter. The original theories of Stevenson, Hubbard, and DeWitt were based on the assumption that the mixture consisted of fully pressure-ionized hydrogen and helium. For the temperatures and pressures found in Saturn and Jupiter, this assumption is now known to be inaccurate, especially for helium (14, 15). Klepeis *et al.* (12) and Pfaffenzeller *et al.* (13) developed mixture models based on density functional theory (DFT). This opens up the possibility of providing an accurate description of electron-ion interactions without assumptions on the extent of ionization. Klepeis *et al.* calculated the enthalpy of mixing at zero temperature from the analysis of crystal structures with different concentrations of helium. Using those enthalpies and the assumption of ideal mixing for the entropy, they obtained a demixing temperature of 15,000 K for $x_{\mathrm{He}} = 0.07$, which suggests that there should be a major phase separation in both Jupiter and Saturn. However, this work neglected both the relaxation of the ionic crystal after the introduction of helium, and disorder characteristic of a fluid. Using first-principles molecular dynamics (FPMD) simulations with the Car-Parrinello technique, Pfaffenzeller *et al.* (13) developed a model including a realistic fluid structure. They performed molecular dynamics (MD) simulations of fluid pure hydrogen and estimated the free energies of a mixture by a reweighting technique. They found a negligible temperature effect on the mixing free energy up to temperatures of 3,000 K and therefore disregarded thermal effects in enthalpies of mixing and used the ideal mixing for the entropy. They obtained immiscibility temperatures too low to allow for differentiation in either Jupiter or Saturn.

In the present work, the temperature, pressure and composition dependence of the enthalpy in hydrogen–helium mixtures is computed with FPMD simulations (see Methods) based on DFT. DFT has become the method of choice in theoretical studies at high pressures, producing sufficiently accurate results for hydrogen and helium (16, 17). We neglect the zero point energy of the ions, which has been shown to be small and will have a negligible effect on the immiscibility temperature within our precision (18). Using thermodynamic integration, we esti-

Author contributions: M.A.M., E.S., D.C., and C.P. designed research; M.A.M. performed research; M.A.M., E.S., D.C., S.H., and K.C. contributed new analytic tools; M.A.M., D.C., and C.P. analyzed data; and M.A.M., E.S., D.C., C.P., S.H., and K.C. wrote the paper.

The authors declare no conflict of interest.

Freely available online through the PNAS open access option.

[1]To whom correspondence should be addressed. E-mail: ceperley@uiuc.edu.

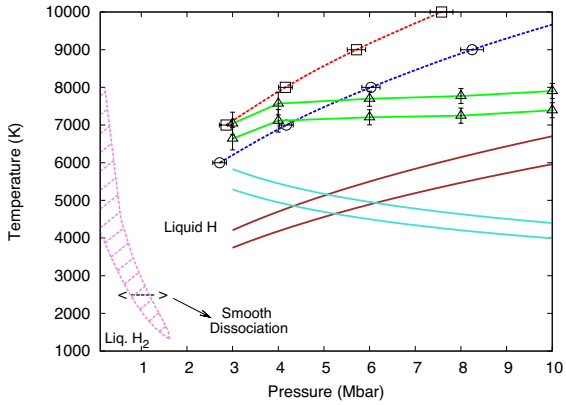

Fig. 1. Schematic phase diagram of hydrogen–helium mixtures at 2 compositions in the relevant range. Immiscibility lines, solid lines; this work, triangles (green, guide to the eye); Pfaffenzeller *et al.* (13), brown; Hubbard-DeWitt (11), turquoise; the latter two are parameterized as in ref. 1. In all three cases, the upper line corresponds to $x_{He} = 0.0847$ and the lower one corresponds to $x_{He} = 0.0623$. Isentropes, dashed lines; Jupiter assuming a composition $x_{He} = 0.07$, squares (red, guide to the eye); Saturn assuming a composition $x_{He} = 0.0667$, circles (blue, guide to the eye). Also shown in the lower left corner is the molecular H_2 dissociation region of the mixture (dashed violet) from refs. 19 and K.C., S. Hamel, T. Ogitsu, F. Gygi, and E.S.; unpublished data.

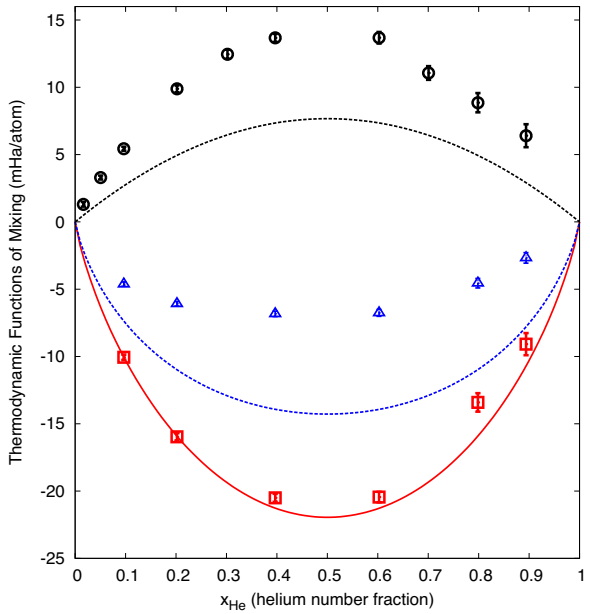

Fig. 2. Internal energy (black open circles), entropy contribution to the free energy (red squares) and Helmholtz free energy (blue triangles) of mixing as a function of the helium number fraction, at the reference point. The red solid line represents the ideal entropy of mixing and the black and blue dashed lines are results from Pfaffenzeller *et al.* (13).

mate the Helmholtz free energy of the mixture and determine the demixing temperature as a function of pressure and composition, thereby avoiding many of the previous assumptions and providing the most accurate prediction of the hydrogen–helium immiscibility, to date. Fig. 1 summarizes the main findings of this work. The isentropes for Jupiter and Saturn determined from our DFT-based equation of state (EOS) are shown along with the temperature of demixing. Overall, we find that the demixing temperature is high enough to support the scenario where helium is partially miscible over a significant fraction of the interior of the Jovian planets, with the corresponding region in Saturn being larger than in Jupiter.

Results and Discussion

We calculated the EOS of the hydrogen–helium system as a function of composition in the temperature range 4,000 to 10,000 K and in the density range 0.3 to 2.7 g/cm^3, by a series of FPMD simulations in the NVT ensemble. We studied 12 different compositions to obtain an accurate interpolation of the energy and pressure. Using the EOS we calculated free energies by integrating along isotherms and isochores. We used the following multistep process to estimate the Gibbs free energy:

1. We computed the free energy of an effective model at the "reference point" (T_{ref} = 10,000 K, r_s = 1.25)* for all 12 compositions (see Methods section). At this point the structure of the liquid mixture can be reasonably well reproduced by simple pair potentials between classical point particles.
2. Using Coupling Constant integration (CCI) (see Methods section), we computed the free energy difference at the reference point between the DFT model and the effective model.
3. Integrating the EOS along constant temperature and constant volume paths, we obtained the free energy difference between the reference point and any other thermodynamic point in the range investigated.
4. Finally, inverting the pressure-volume relations we obtained the Gibbs free energy of mixing as a function of pressure, temperature and composition.

Fig. 2 shows the Helmholtz free energy of mixing as a function of helium number fraction (x_{He}) at the reference point and its energetic and entropic contributions. Fig. 2 clearly shows, at least at the reference point, that the ideal mixing assumption to describe the entropy of mixing is very accurate for $x_{He} \leq 0.2$ but becomes less accurate for larger helium concentrations. The reason for this behavior is that the local environment of a proton in the low hydrogen concentration region is very different from the one it experiences in the metallic state of the pure system (see the discussion of pair correlations below). However, the inert character of helium makes it insensitive to change in the local environment in the low helium concentration region. In Fig. 2, we compare our results to the prediction of Pfaffenzeller *et al.* (13) who neglected thermal effects in the internal energy of mixing and used the ideal mixing law. The neglect of thermal effects in the internal energy results in a too large and negative mixing free energy. Although it is true that the thermal effects are probably negligible at 3,000 K, at this temperature the system is strongly immiscible so that the reweighting procedure used in (13) to estimate those effects is likely to be inaccurate.

In Fig. 3 we present the calculated Gibbs free energy of mixing as a function of composition; in Fig. 3*A* several pressures are shown at a temperature of 8,000 K, whereas in Fig. 3*B*, several temperatures are shown at a pressure of 10 Mbar. Note that at 8,000 K, pressure has a small effect on the mixing free energy for low helium concentrations. In particular, a minimum in the free energy located at $x_{He} \approx 0.1$ is observed for all pressures investigated; this implies a stable mixture at this concentration. However, pressure has a strong effect at higher helium concentrations where, at a temperature of 8,000 K, an increase from 4 to 10 Mbar eliminates the second minimum in the free energy

*r_s is the Wigner–Seitz radius and defines the electronic density.

ASTRONOMY

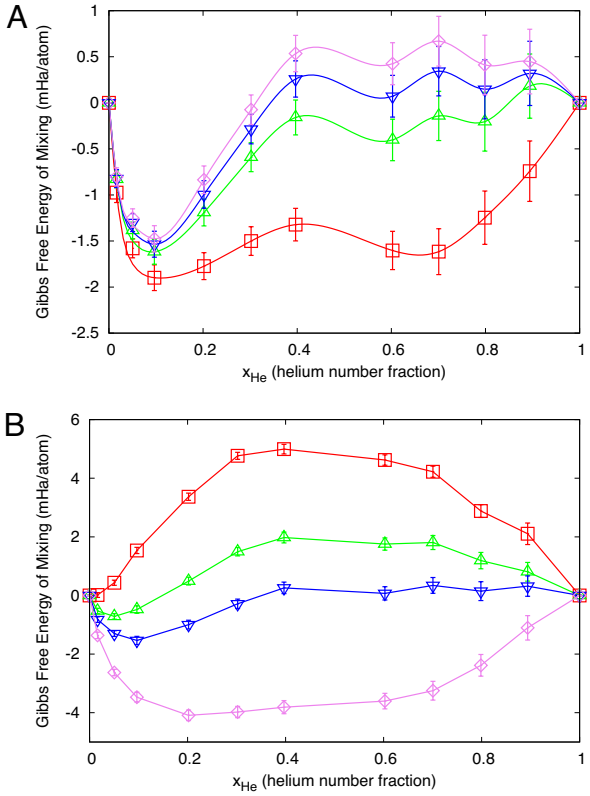

Fig. 3. The Gibbs free energy of mixing as a function of composition. (*A*) Data at 8,000 K for several pressures: 4 Mbar (red squares), 8 Mbar (green triangles), 10 Mbar (blue inverted triangles) and 12 Mbar (violet diamonds). (*B*) Data at $P = 10$ Mbar for several temperatures: 5,000 K (red sqaures), 7,000 K (green triangles), 8,000 K (blue triangles), and 10,000 K (violet inverted triangles). Results of calculations are shown as symbols and error bars; solid lines are guides to the eye only.

curve[†]. The common tangent construction is used to estimate the demixing temperatures. For points where no minima at high helium concentration is evident, we have assumed complete immiscibility. From the free energy plots of Fig. 3 it is clear that this assumption will have a negligible effect on the location of the minimum at low helium concentration. As shown in of Fig. 3*B*, temperature has a strong effect on the mixing free energy, and hence, on immiscibility. An increase in temperature from 7,000 to 9,000 K (data not shown in the figure) is enough to change the concentration of helium at the saturation point from 5% to 15%.

Fig. 4 shows the demixing temperature versus composition for pressures ranging from 4 to 12 Mbar. Also shown are the results from the previous DFT-based calculations (12, 13). As suggested by the free energy curve in Fig. 3, pressure has only a moderate effect on the immiscibility process. For a fixed helium fraction, the demixing temperature changes by ≈500 K in a pressure range of 8 Mbar for the relevant concentrations (5% to 10%).

Recent first-principles studies of pure helium have examined the effect of temperature on band gap closure, suggesting that metallization in helium can occur at much smaller pressures than expected (14). To examine the nature of helium in the mixtures, we calculated the electronic conductivity of pure helium, using the Kubo–Greenwood

[†]We have concentrated the majority of our simulation efforts on the small x_{He} part of the phase diagram more relevant to planetary models. Quantitative prediction of miscibility at large x_{He} is more difficult because of the smaller mixing free energy involved and will require additional investigations.

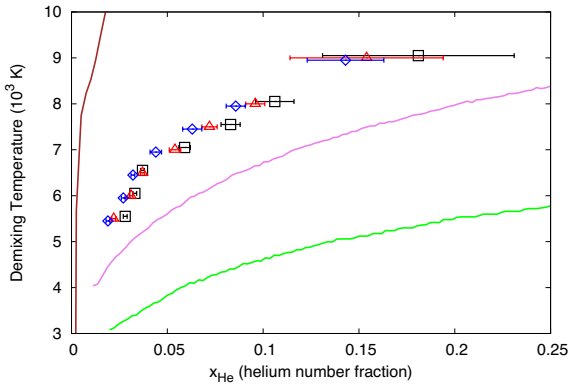

Fig. 4. Demixing transition temperatures as a function of helium number fraction, for several pressures: 4 Mbar (black squares), 8 Mbar (Δ, red), 12 Mbar (blue diamonds). Continuous lines are the results of ref. 12 for 10.5 Mbar (brown) and ref. 13 for 8 (green) and 10 (violet) Mbar.

approach within DFT[‡] and obtained values well below 100 $(\Omega\cdot\text{cm})^{-1}$, even at the highest temperature and density reported here. Furthermore, in the recent work by Stixrude *et al.* (14), for $\rho \approx 5.4$ g/cm^3 the band gap is found to close at temperatures beyond 20,000 K, well above our estimated demixing temperature. Metallization should enhance helium solubility, but as clearly shown here, for the pressures relevant to the modeling of Jovian planets, immiscibility occurs at temperatures well below those required to produce ionization in helium (15); fully ionized models are not appropriate for describing the pressure dependence of the demixing temperature. At pressures much higher than those examined here, metallization of helium will play an important role and should produce significant changes to the pressure dependence of the immiscibility temperature.

The structure of hydrogen is strongly influenced by the helium concentration. Although at low x_{He} hydrogen is in the monoatomic fully ionized state, an effective proton-proton attraction reminiscent of the molecular bonding develops upon increasing x_{He}, even at very high pressures and temperatures. Fig. 5 shows several hydrogen-hydrogen radial distribution functions for mixtures with various helium concentrations, for temperatures of 8,000 K and 10,000 K and electronic densities given by $r_s = 1.05$ and $r_s = 1.25$ respectively. A molecular-like peak builds up smoothly as $x_{He} \to 1$. Under these conditions, helium is not ionized; this inhibits the delocalization of the hydrogenic electrons, enhancing the formation of weak molecular bonds. Because of the very low proton concentration, the observed proton-proton correlation can be interpreted as resulting from an effective Morse potential. Fitting $-\log(g_{pp}(r))/T$ to this analytic form yields well depth parameters ≈300 times smaller than in an isolated hydrogen molecule. Such weak attraction gives proton pairs with short lifetimes, as also inferred from direct inspection of the MD trajectories. A similar stabilization of molecular hydrogen by helium, but at much lower temperature and density, has been reported close to the dissociation regime in pure hydrogen (19).

The computed demixing temperatures found here have important implications for the study of the interior structure of hydrogen rich planets, especially Saturn. Our results support the scenario where helium becomes partially miscible in the intermediate layers of the planet, with the excess helium falling toward the core through gravitational differentiation. This mechanism has been proposed to explain the high surface temperatures observed in Saturn (2) and the depletion of helium

[‡]These calculations were performed on 15 de-correlated configurations from a FPMD trajectory, where we employed a 6×6×6 Monkhorst-Pack k-point grid.

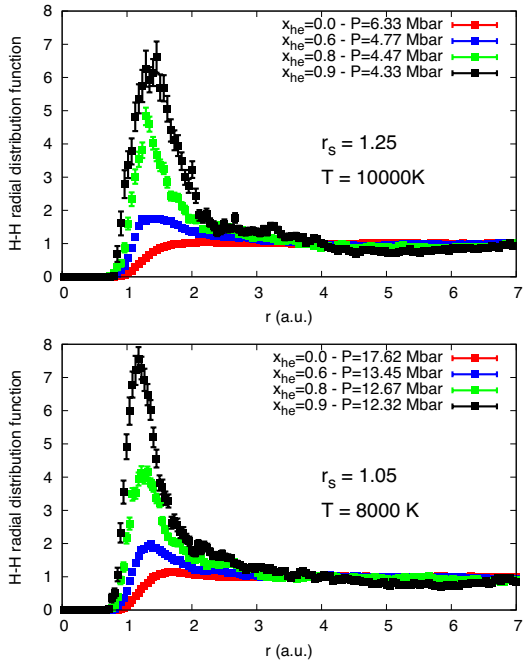

Fig. 5. The effect of increasing concentrations of helium on the proton-proton radial distribution function at $r_s = 1.25$ (*Upper*) and $r_s = 1.05$ (*Lower*).

in the atmosphere. Whether the immiscible region will be large enough to explain all of the observed properties of the planet remains an open question, but the current work represents a clear indication that a correct description should include phase separation. In general, DFT represents a large modification to the existing interior models, based mostly on the Saumon, Chabrier, Van Horn EOS (20) (SCVH). As recently shown by Militzer *et al.* (21), a combination of the DFT EOS with the inclusion of nonideal effects in the mixing leads to isentropic Jupiter models that are cooler than the corresponding SCVH ones by ≈1,000–2,000 K at high pressures. Even though the results reported here suggest that the interior model cannot be assumed to be isentropic, nonadiabatic models based on DFT including nonideal effects should produce qualitatively similar results to those found by Militzer. To give an indication of the general changes expected with the proper inclusion of these effects, we calculated the SCVH isentropes (corresponding to the interpolated EOS) of Jupiter and Saturn, using our DFT-based EOS. The results are shown in Fig. 1, where we have assumed fixed helium concentrations of $x_{\mathrm{He}} = 0.07$ for Jupiter and $x_{\mathrm{He}} = 0.0667$ for Saturn.

At low density ($\rho \leq 0.3$ g/cm^3), before the dissociation of hydrogen plays a significant role, the pressures produced by the SCVH model are in good agreement with DFT. To compare the entropy of both models at low density, and assess the agreement of the isentropes there, we performed simulations with $x_{\mathrm{He}} = 0.0667$ following a path through the region of miscibility starting from the reference point and ending at a density of $\rho = 0.3$ g/cm^3, where we simulated several temperatures. Then, using thermodynamic integration, we calculated the free energy and the entropy at the point where the SCVH planetary isentrope crosses this density. We obtain entropies that agree with the SCVH model to within 1.5%. With the onset of dissociation for higher densities, the isentrope from the SCVH model deviates significantly from DFT results. Although the possible immiscibility puts in question the use of an isentropic model for the interior of Saturn, our analysis provides an estimate of the magnitude of changes to the SCVH based models. The present results are in good agreement with those reported by Militzer (21) for the Jupiter isentrope. As can be seen, the portion of the interior of Saturn corresponding to pressures between 1.5 to 5.5 Mbar should be inside the immiscible region, with the stable concentration of helium depending on pressure.

Conclusion

In summary, we have carried out an extensive investigation of the properties of hydrogen–helium mixtures at pressures and temperatures that are relevant to the interior of Jupiter and Saturn, using state-of-the-art ab initio simulation methods. By using a combination of first-principles molecular dynamics simulations within DFT and thermodynamic integration techniques, we have accurately determined the Gibbs free energy of mixing over a wide range of density, temperature and composition. Our work differs from previous investigations in that it does not rely on any assumptions about mixing functions. Our simulation results are consistent with the idea that a large portion of the interior of Saturn has conditions such that hydrogen and helium phase separate; this can account for the apparent discrepancy between the current evolution models for Saturn and observational data.

The accuracy of the present results is primarily limited by the approximate density functional used. Quantum Monte Carlo calculations for helium and hydrogen do not require assumptions about the electron correlation, pseudopotentials and zero-point energy of the nuclei. A systematic investigation of the correction to DFT, using the Quantum Monte Carlo method described in ref. 17 is in progress.

Methods

First Principles Calculations. The FPMD simulations performed in this work were based on Kohn-Sham density functional theory, using the Perdew–Burke–Ernzerhof (PBE) exchange-correlation functional. We used Born-Oppenheimer MD (BOMD) within the NVT-ensemble (with a weakly coupled Berendsen thermostat), as implemented in the Qbox code (http://eslab.ucdavis.edu/software/qbox). We used a Hamman type (22) local pseudopotential with a core radius of $r_c = 0.3$ au to represent hydrogen and a Troullier–Martins type (23) nonlocal pseudopotential with *s* and *p* channels and $r_c = 1.091$ au to represent helium. Tests have established the accuracy of the hydrogen and helium pseudopotentials over the relevant pressure range, up to 13 Mbar[§]. A plane wave energy cutoff of 90 Ry was used for $r_s \geq 1.10$ and of 115 Ry for $r_s < 1.10$. Empty states were included with an electronic temperature set to the ionic temperature. To integrate the equation of motion during the dynamics we used a time step of 8 a.u.

We used 250 electrons for $r_s < 1.65$ and 128 electrons otherwise. The Brillouin zone was sampled at the Γ-point. To reduce systematic effects and to get accurate pressures, we added a correction to the EOS designed to correct for the plane wave cutoff and the sampling of the Brillouin zone. To compute this, we studied 15–20 configurations at each density and composition by using a $4 \times 4 \times 4$ grid of k-points with a plane-wave cutoff of at least 300 Ry. The actual plane-wave cutoff used depended on density and was chosen to achieve full convergence in the energy and pressure.

For the calculation of the EOS, we studied 4 temperatures, 6 densities and 12 compositions for a total of 288 simulations. We also performed 15 simulations to extend the calculation of the free energy to low density. For the integration of the free energy we studied 8 compositions, each one required 5 additional calculations. In the case of the BOMD simulations, we first equilibrated the system, using a suitable effective model and subsequently allowed 300–500 time steps of equilibration with DFT, averages were accumulated for ≈2,000 time steps. For the thermodynamic integration, the simulations were first equilibrated with the effective potential and subsequently allowed to equilibrate for 1,000–2,000 time steps, using the mixed DFT-effective potential, averages were calculated for 12,000–18,000 time steps. In both cases, this was sufficient for accurate results. In total, the

[§]The sensitivity of the free energy to the choice of the helium pseudopotential was estimated by comparing the enthalpy of 20 ionic configurations with a Hamman type local pseudopotential with r_c=0.218 au for helium and a plane wave cutoff of 450 Ryd. The difference in the free energy of mixing is estimated to be 0.1 mH/atom, this is smaller than the error bars reported in Fig. 3.

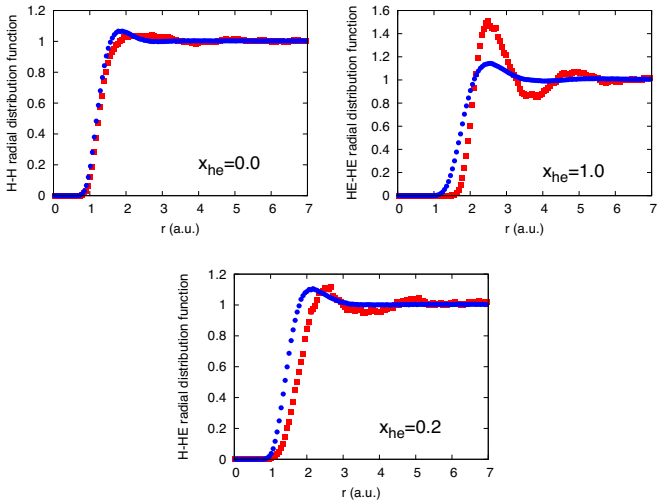

Fig. 6. Comparison of several radial distribution functions between the effective (blue) and the DFT (red) system at the reference point. We choose Yukawa pair potentials to calculate the Helmholtz free energy at the reference point.

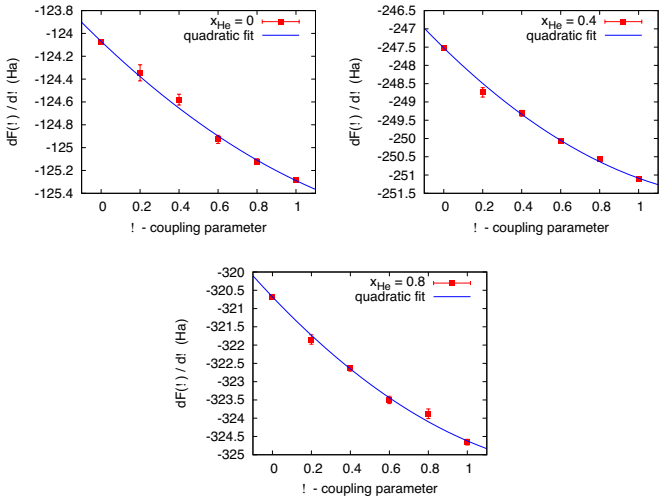

Fig. 7. Results of the simulations for the mixed effective-DFT potential used in the CCI of the free energy difference for several compositions. As can be seen, the results depend smoothly on the coupling parameter and no singular behavior is observed close to the endpoints.

simulations reported here used approximately 3 million CPU hours on a large Opteron-based Linux cluster.

Coupling Constant Integration. CCI allows us to calculate the difference in free energy between systems with different interacting potentials. For a system described by the potentials V_1 and V_2:

$$V(\lambda) = \lambda V_1 + (1-\lambda)V_2 \qquad [1]$$

$$F_1(T,V,N) - F_2(T,V,N) = \int_0^1 \frac{dF(\lambda)}{d\lambda}\, d\lambda$$

$$= \int_0^1 \langle V_1 - V_2 \rangle_{T,V,N,\lambda}\, d\lambda, \qquad [2]$$

where $\langle\rangle_{T,V,N,\lambda}$ represents a canonical average with the potential $V(\lambda)$. Any functional form of the two potentials is formally allowed in Eq. **1**, but the use of similar potentials makes the integration of the free energy difference considerably easier in practice.

To represent the interaction between the atoms in the classical system, we used reflected Yukawa pair potentials:

$$V(r) = \begin{cases} a\left(\dfrac{e^{-br}}{r} + \dfrac{e^{-b(L-r)}}{(L-r)} - 4\dfrac{e^{-bL/2}}{L}\right) & r \le L/2, \\ 0 & r > L/2, \end{cases} \qquad [3]$$

where a, b, and L are free parameters and depend on the identity of the atoms¶. As shown in Fig. 6, this potential was found to exhibit similar pair correlations as the DFT model for pure hydrogen, but was not as good for helium. We choose the pair potentials such that the effective model was fully miscible at the reference point to avoid crossing a phase line during the integration. We computed the Helmholtz free energy of the effective model, using CCI and classical MC simulations, with the second potential set to zero in Eq. **1**. From this we determined the free energy of the effective model because the free energy of the noninteracting model is known. We also calculated the free energy by integrating the pressure from the reference volume to a volume large enough that the system is ideal; the pressures were obtained by a series of classical MC simulations. Both approaches produced agreement within noise.

The free energy difference between the DFT-based and the effective models was calculated using the CCI approach. Fig. 6 shows a comparison of the radial distribution functions of the effective and DFT models for selected compositions at the reference point. To compute the required canonical averages, we used a Hybrid Monte Carlo (HMC) algorithm (24), which allows for an efficient sampling of large systems with many-particle moves. HMC results in exact sampling of the canonical ensemble without time step errors. In this work, the HMC approach was found to be as efficient as MD if the time step is chosen carefully. Fig. 7 shows the results of the HMC simulations for several compositions. The curves are smooth. This is the only requirement to justify the procedure. Fig. 2 summarizes the main results of the computations at the reference point.

ACKNOWLEDGMENTS. We thank D.J. Stevenson and N.W. Ashcroft for useful comments. C.P. thanks the Institute of Condensed Matter Theory at the University of Illinois at Urbana–Champaign for a short-term visit. This work was supported by the Department of Energy National Nuclear Security Administration (M.A.M.); Department of Energy under Contract DOE-DE-FG52-06NA26170 (to D.M.C.); Ministero dell'Istruzione, dell'Università e della Ricerca Grant PRIN2007 (to C.P.). Extensive computational support was provided by the Livermore Computing facility. This work was partly performed under the auspices of the U.S. Department of Energy by Lawrence Livermore National Laboratory under Contract DE-AC52–07NA27344.

¶We used $a_H = a_{He} = a_{H-He} = 1$, $L_H = L_{He} = L_{H-He} = 8$ a.u., $b_H = 2.5$ a.u., $b_{He} = 1.2$ a.u. and $b_{H-He} = 1.9$ a.u.

1. Fortney JJ, Hubbard WB (2003) Phase separation in giant planets: Inhomogeneous evolution of Saturn. *Icarus* 164:228–243.
2. Fortney JJ, Hubbard WB (2004) Effects of helium phase separation on the evolution of extrasolar giant planets. *Astrophys J* 608:1039–1049.
3. Guillot T (2005) The interiors of giant planets: Models and outstanding questions. *Annu Rev Earth Planet Sci* 33:493–530.
4. Hubbard WB, Burrows A, Lunine JI (2002) Theory of giant planets. *Annu Rev Astron Astrophys* 40:103–136.
5. Hubbard WB, et.al (1999) Comparative evolution of Jupiter and Saturn. *Planet Space Sci* 47:1175–1182.
6. Salpeter EE (1973) On convection and gravitational layering in Jupiter and in stars of low mass. *Astrophys J* 181:L83–L86.
7. Stevenson DJ (1975) Thermodynamics and phase separation of dense fully ionized hydrogen–helium fluid mixtures. *Phys Rev Condens Matter B* 12:3999–4007.
8. Stevenson DJ, Salpeter EE (1977) Phase diagram and transport properties for hydrogen–helium fluid planets. *Astrophys J Suppl* 35:221–237.
9. Stevenson DJ, Salpeter EE (1977) Dynamics and helium distribution in hydrogen–helium fluid planets. *Astrophys J Suppl* 35:239–261.
10. Straus DM, Ashcroft NW, Beck H (1977) Phase separation of metallic hydrogen–helium alloys. *Phys Rev B* 15:1914–1928.

11. Hubbard WB, DeWitt HE (1985) Statistical mechanics of light elements at high pressure. VII - A perturbative free energy for arbitrary mixtures of H and He. *Astrophys J* 290:388–393.
12. Klepeis JE, Schafer KJ, Barbee TW, Ross M (1991) HydrogenÐ helium mixtures at megabar pressures—Implications for Jupiter and Saturn. *Science* 254:986–989.
13. Pfaffenzeller O, Hohl D, Ballone P (1995) Miscibility of hydrogen and helium under astrophysical conditions. *Phys Rev Lett* 74:2599–2602.
14. Stixrude L, Jeanloz R (2008) Fluid helium at conditions of giant planetary interiors, *Proc Natl Acad Sci USA* 105:11071–11075.
15. Stevenson DJ (2008) Metallic helium in massive planets, *Proc Natl Acad Sci USA* 105:11035–11036.
16. Bonev SA, Schwegler E, Ogitsu, Galli G (2004) A quantum fluid of metallic hydrogen suggested by first-principles calculations. *Nature* 431:669–672.
17. Pierleoni C, Delaney KT, Morales MA, Ceperley DM, Holzmann M (2008) Trial wave functions for high pressure metallic hydrogen. *Comput Phys Commun* 179:89–97.
18. Pierleoni C, Ceperley DM, Holzmann M (2004) Coupled Electron-Ion Monte Carlo calculations of dense metallic hydrogen. *Phys Rev Lett 93*: 146402:1–4.
19. Vorberger J, Tamblyn I, Militzer B, Bonev SA (2007) Hydrogen-helium mixtures in the interiors of giant planets. *Phys Rev B* 75:024206.
20. Saumon D, Chabrier G, Van Horn HM (1995) An equation of state for low-mass stars and giant planets. *Astrophys J Suppl S* 99:713–741.
21. Militzer B, Hubbard WB, Vorberger J, Tamblyn I, Bonev SA (2008) A massive core in jupiter predicted from first-principles simulations. *Astrophys J Lett*, in press.
22. Hamman DR (1989) Generalized norm-conserving pseudopotentials. *Phys Rev B* 40:2980–2987.
23. Troullier N, Martins JL (1991) Efficient pseudopotentials for plane-wave calculations. *Phys Rev B* 43:1993–2006.
24. Mehlig B, Heermann DW, Forrest BM (1992) Hybrid Monte Carlo method for condensed-matter systems. *Phys Rev B* 45:679–685.